HSD Map Transformation Mechanization

E. A. O'Hern* and T. C. Lu†
North American Rockwell Corporation, Anaheim, Calif.

This paper treats the development of a computer software mechanization to accurately and efficiently drive and annotate a projected map in response to input latitude and longitude information. General system requirements are outlined, emphasizing the need for transforming earth location (latitude, longitude) to map coordinates (X, Y) for all required scales and latitude regions for a Lambert Conformal chart projection, in such manner to provide required accuracy while minimizing computational impact. The development of a new transformation mechanization is outlined. Final configuration is shown to be selectable as a function of system accuracy requirements. System error analysis procedure is described. Analysis results, showing effects of mechanization equation configuration map scales, and map regions are presented. The resulting computer software mechanization is described, indicating the relative reduction in memory and duty cycle requirements. Program advantages of the application of computer systems engineering to mechanization problems are noted.

I. Introduction

A CENTRAL objective of the modern avionic system is to promote the role of the pilot as mission director by providing easily assimilated situation information while removing the requirement for menial manipulative tasks. The Horizontal Situation Display (HSD), featuring a roller-map or projected map capability, is clearly aimed toward filling this role. It removes the requirement for knee-pad map organization and reflects a plan view of current geographic status.

It is natural that progressively more information finds its way to this situation display, so that strip roller maps have evolved to full two-dimensional map drives, directly interfaced with the airborne navigation system. Further, advanced electro-optical techniques make possible not only rotated projections of a map image, but also projections of symbols and characters whose precise positions correspond to special points of interest on the map (destinations, fixpoints, etc.).

As a consequence of this greater dependence placed on the HSD, greater precision is naturally required for map drive, rotations, and symbol positioning. A critical need, then, is the mechanization of an accurate transformation from Earth position (latitude, longitude on a spheroid) to corresponding map position (Cartesian x, y on a plane). This paper deals with one of the most commonly used (by the map maker) transformations, the Lambert Conformal.

Inasmuch as a straightforward software implementation of the complete Lambert Conformal transformation equations as normally provided would appear to inflict computer memory and duty cycle demands approaching that of a simple inertial navigation system, a software system engineering study was undertaken to develop a simplified mechanization approach that would provide acceptable accuracy for all anticipated map projections.

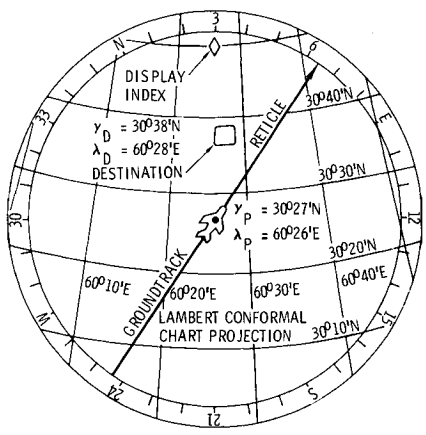

Fig. 1 HSD north-up display, magnetic variation 30 west and groundtrack 35 east.

II. Functional Requirements

Purpose

The primary purpose of a typical HSD mechanization is to display, in conjunction with the HSD hardware, the following superimposed images on a CRT viewing screen: 1) a portion of an Aeronautical Navigation Chart with the aircraft present position latitude and longitude at the viewing screen center; 2) a Compass Rose indicating the Earth magnetic orientation—north, south, east, and west; 3) a Groundtrack Reticle indicating the aircraft ground velocity vector direction and sense; and 4) symbols locating the points of interest, e.g., destination, fixpoint, etc. The display tells where the aircraft is, where its destination is, and in what direction it is flying.

A spheroidal Earth model, which is characterized by an equatorial radius and an Earth eccentricity, is employed. Figure 1 illustrates a north-up display of the Lambert Conformal conic projection of the spheroidal Earth, indicating the following parameter values: 1) aircraft present position latitude of 30° 27′N, 2) aircraft present position longitude of 60° 26′E, 3) magnetic variation of 30°W, 4) groundtrack of 35°E, 5) the destination latitude of 30°38′N, 6) the destination longitude of 60°28′E. The parallels and meridians on the Earth are represented by the concentric circular arcs and radial lines, respectively, on the display in Fig. 1.

Presented as Paper 69–987 at the AIAA Aerospace Computer Systems Conference, Los Angeles, Calif., September 8–10, 1969; submitted September 15, 1969; revision received December 29, 1969. H. M. Gomes provided FORTRAN Programs.

* Chief Scientist, F-111 Avionics, Autonetics Division. Member AIAA.

† Technical Staff, Avionics and Sensors Division, Autonetics Division. Member AIAA.

Sequential Events

The block diagram shown in Fig. 2 presents the HSD sequence of functional events for generating and displaying an Aeronautical Chart on a CRT viewing screen from the HSD mechanization point of view.

Earth

The mathematical model of the Earth used for the mechanization is a spheroid which is characterized by two parameters: 1) semimajor axis or equational radius (a = 6,378,388.0 m); 2) eccentricity (ϵ = 0.081,991,89).

Lambert Conformal projection

Lambert Conformal projection is a conformal transformation, i.e., the transformation of the space surface of the Earth into a plane surface such that the scale is uniform in all directions at any point. The Lambert Conformally-transformed plane surface (developed in more detail in Sec. III) consists of arcs of concentric circles to represent the parallels (constant-latitude lines) and radial lines emitting from the center of the circles to represent the meridians (constant-longitude lines).

Aeronautical chart

An Aeronautical chart is the Lambert Conformal projection of a portion of the Earth at a reduced scale. The chart scales, k_{cs}, relating map dimensions to corresponding Earth dimensions, commonly used are $1{:}0.25 \times 10^6$, $1{:}0.50 \times 10^6$, $1{:}1.00 \times 10^6$, $1{:}2.00 \times 10^6$, and $1{:}5.00 \times 10^6$. The physical size of an Aeronautical chart is about 57.5 in. by 42.0 in. in width and height, respectively. Thus, the portion of the Earth surface that can be shown on a chart depends upon the chart scale.

Transparency

The transparency, or Chart Film Transparency, is a reproduction of an Aeronautical chart at a fixed reduction of k_r. It provides a map of manageable size and permits projection of the chart image on the viewing screen for display. The physical size of a transparency depends on the value of k_r.

Optics

Optics are used a) to project and magnify (k_m) the transparency on the viewing screen for display (resulting scale = $k_m \times k_r \times k_{cs}$) and b) to rotate the chart image.

x and y servo drives

The transparency roll is driven by the x and y servo drives, so that 1) the selected transparency (several may be available) is shown and 2) the transparency may be shifted so that aircraft present position is centered on the circular viewing screen.

Symbol drives

It is often desirable to position symbols representing points of interest relative to the map for display. This projection can be made relative to the map prior to optical projection, or relative to the resulting display orientation.

Computational Tasks

The computational tasks required to perform the HSD functions are mainly as follows.

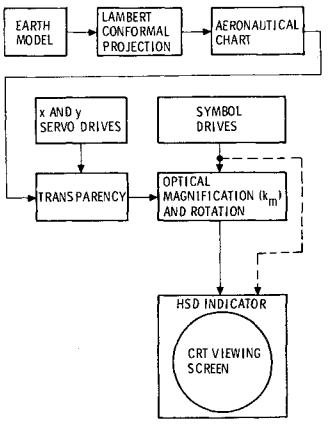

Fig. 2 Sequence of HSD functional events.

Coordinate transformation

A coordinate transformation of Earth curvilinear coordinates, latitude and longitude (γ and λ), to the rectilinear coordinates x and y is needed to provide commands to the x and y servo drives. Preferably, the same transformation computation is applicable to both the aircraft present position and the points of interest.

Means of identifying charts

Generally, transparencies of numerous charts are available for selection. Means of identifying each one is needed, so that proper one can be selected.

Means for introducing parametric values

For each new transparency selected, a corresponding set of parameters is needed, so that there is one-to-one correspondence between the transparency selected and resulting coordinate transformation computation. The objective here is to provide adequate accuracy with simple coordinate transformation computation and a minimum of stored parameters.

III. Mechanization Development

Lambert Conformal Conic Projection

A highly desirable property of any navigation map transformation is conformality. This condition requires that the map scale at any given point is equal in all directions, thus preserving angular (e.g., bearing) significance when viewing the map. As an example, the curvilinear coordinates γ, λ of the spheroid (Fig. 3) can be mapped into Cartesian coordinates τ, λ on a plane such that the meridians are parallel (Fig. 4). Conformality is established by stretching the distance between parallels with increasing latitude so that the scale along the meridians is increased to exactly match the increasing scale along the parallels. The "stretching" rela-

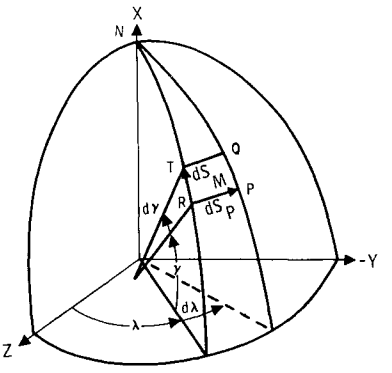

Fig. 3 Curvilinear coordinates γ and λ.

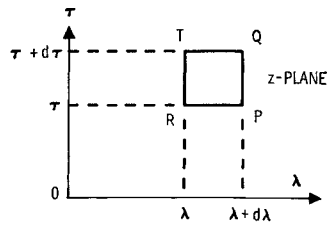

Fig. 4 Mercator projection, Cartesian coordinates τ and λ.

tionship is found to be

$$\tau = \ln\left[\left(\frac{1 - \epsilon \sin\gamma}{1 + \epsilon \sin\gamma}\right)^{\epsilon/2} \tan\left(\frac{\pi}{4} + \frac{\gamma}{2}\right)\right] \qquad (1)$$

and γ and τ are called geodetic and isometric latitudes, respectively.

In the process of this transformation, an infinitesimally small quadrilateral space surface RTQP in Fig. 3 is transformed into a small quadrilateral plane surface RTQP in Fig. 4. This transformation is referred to as a Mercator Projection.

Note that the rate of change of scale becomes larger as latitude increases. Inasmuch as another desirable property of navigation map transformations is that the map scale be nearly equal over a large viewing area, improvement is sought for nonequatorial latitudes.

Referring to Fig. 5, it can be seen that, if the plane map surface is taken as the developed cone tangent to the spheroid at the latitude of interest, no additional stretching along the meridians is necessary at the point of tangency because the rate of shortening of parallels with latitude increase is equal for both spheroid and plane surfaces. The scale variation is small in the region near this central latitude γ_o. The developed secant cone, Fig. 6, is typically defined by two standard parallels of secant intersection, γ_1 and γ_2. When this cone is thereby established, and the conformality constraint retained, the transformation relationships (defining the Lambert Conformal projection) become

$$x = r \sin l\lambda, \quad y = r \cos l\lambda, \quad r = Ke^{-l\tau}$$

$$l = \ln(N_1 \cos\gamma_1/N_2 \cos\gamma_2)/(\tau_2 - \tau_1) = \sin\gamma_0$$

$$K = N_1 \cos\gamma_1 \, e^{l\tau_1}/l$$

$$N = a(1 - \epsilon^2 \sin^2\gamma)^{-1/2} \qquad (2)$$

$$= \text{radius of curvature along parallel}$$

$$R = a(1 - \epsilon^2)(1 - \epsilon^2 \sin^2\gamma)^{-3/2}$$

$$= \text{radius of curvature along meridian}$$

γ_1, γ_2 = latitudes at the two standard-parallels where the transformation scale factor is unity,[1] γ_o = equivalent parallel for corresponding one standard parallel projection where τ is as given in Eq. (1). In this conformal transformation, the small surface RTQP in Figs. 3 and 4 is transformed into a small quadrilateral plane surface R′T′Q′P′ in Fig. 6.

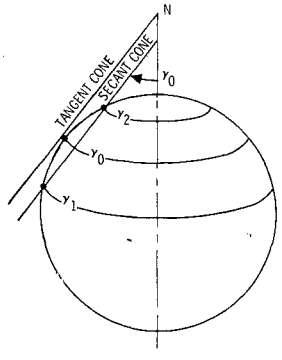

Fig. 5 Tangent and secant cones.

Mechanization Objective

Factors

Three primary factors to be considered during the mechanization development are 1) accuracy, 2) computer storage, and 3) computer duty cycle. The objective is to develop a simple mechanization which provides adequate accuracy with reasonable computer storage and duty cycle requirements compatible with the computer capability.

Map radius equation

As shown in Eqs. (2), the Lambert Conformal transformation from the curvilinear coordinates γ and τ into the rectangular Cartesian coordinates x and y requires the computer computation of the map radius $r = Ke^{-l\tau}$ where again

$$\tau = \ln\left[\left(\frac{1 - \epsilon \sin\gamma}{1 + \epsilon \sin\gamma}\right)^{\epsilon/2} \tan\left(\frac{\pi}{4} + \frac{\gamma}{2}\right)\right]$$

The computer storage and duty cycle required for computing the map radius using these equations was found to be excessive.

Estimate of map radius accuracy requirements

An estimate is made in the following to provide an order of magnitude indication pertaining to the map radius accuracy requirement. Let r = Lambert projection map radius = semimajor axis of Earth = $a = 2.5 \times 10^8$ in.; then r_c = chart map radius = $k_{cs}a$. Table 1 lists the map radius accuracy required to provide a relative display accuracy of 0.5% for a display screen diameter of 6 in. It indicates that a map radius mechanization accuracy in the order of 0.003% is required.

Mechanization Approaches

Four mechanization approaches to the map radius equation have been considered: 1) series expansion (wherein series for the exponential, logarithm, and exponential functions are employed); 2) empirical curve fitting polynominal (wherein r and τ are expressed as power series functions of τ and γ, respectively); 3) reference point integral [where r is expressed as a map reference r plus the integral of computed differentials $dr = (dr/d\gamma)\, d\gamma$]; 4) reference point differential (wherein r is expressed as a map reference r plus an increment Δr given as a Taylor's series expansion of $\Delta\gamma$).

The computer storage and duty cycle requirements for using these four approaches based on the same degree of accuracy have been estimated and are listed in Table 2. As a point of reference, approach 2 requires nearly 3 times the computer memory as does approach 4 for transformation computations (plus 25% more memory for map parameter storage), and utilizes approximately 4 times the duty cycle. Inasmuch as the reference-point differential approach appears most promising, it will be discussed in greater detail in the following sections.

Table 1 Map radius mechanization accuracy requirement

Chart scale k_{cs}	Chart map radius r_c, in.	Chart map radius accuracy for 0.5% relative display error $e_{r_c}/r_c = 0.03/r_c$, %
$1{:}0.25 \times 10^6$	1000	0.003
$1{:}0.50 \times 10^6$	500	0.006
$1{:}1.00 \times 10^6$	250	0.012
$1{:}2.00 \times 10^6$	125	0.024
$1{:}5.00 \times 10^6$	50	0.060

Derivation of Reference-Point Conformality Equations

The expression for the derivative terms $d^i r/d\gamma^i$, in the Taylor series is to be derived by using the conformality property. Figures 3 and 6 present a spheroidal Earth and its Lambert Conformal projection. At a reference point R of map radius r_R, the conformal transformation scale factors along the earth parallel and meridian are from inspection as follows:

$$k_p = dS'_p/dS_p = rld\lambda/N\cos\gamma d\lambda$$
$$k_M = dS'_M/dS_M = -dr/Rd\gamma \tag{3}$$

The conformality conditions requires that

$$k_p = k_M \tag{4}$$

Substituting Eqs. (3) into Eq. (4) results in

$$dr/d\gamma = -Rrl/N\cos\gamma$$
$$= -(1-\epsilon^2)(1-\epsilon^2\sin^2\gamma)^{-1}/\cos\gamma rl$$
$$\cong -l(1/\cos\gamma - \epsilon^2\cos\gamma)r \tag{5}$$

Equation (5) is a key differential equation to the HSD mechanization. It provides the computation of the rate of change in the Lambert Projection map radius with respect to the change in the earth geodetic latitude. Successive differentiation of Eq. (5) and approximation result in

$$d^2r/d\gamma^2 = dr/d\gamma[(\sin\gamma - l)/\cos\gamma] \tag{6}$$

$$\frac{d^3r}{d\gamma^3} = \frac{dr}{d\gamma}\left[1 + \frac{2(\sin\gamma - l)(\sin\gamma - l/2)}{\cos^2\gamma}\right] \tag{7}$$

$$d^4r/d\gamma^4 = (dr/d\gamma)[5(\sin\gamma - 0.8l)/\cos\gamma + 6(\sin\gamma - l)(\sin\gamma - l/2)/\cos^3\gamma \times (\sin\gamma - l/3)] \tag{8}$$

With the aid of Eqs. (5) and (8), the Taylor's series expression for the Lambert projection radius at any latitude γ with respect to that at the reference latitude γ_R is given as follows:

$$r = r_R + \Delta r \tag{9}$$

where

$$\Delta r = \sum_{n=1}^{\infty} \frac{(d^n r)}{d\gamma^n{}_R}\frac{(\Delta\gamma)^n}{n!} \tag{10a}$$

$$\Delta\gamma = \gamma - \gamma_R \text{ rad} \tag{10b}$$

Equation (10a) is rewritten as follows:

$$\Delta r = a\Delta\gamma[1 + b\Delta\gamma + c(\Delta\gamma)^2 + d(\Delta\gamma)^3 + \ldots] \tag{11}$$

where

$$a = -l(1/\cos\gamma_R - \epsilon^2\cos\gamma_R)r_R \tag{12a}$$
$$b = (\sin\gamma_R - l)/2\cos\gamma_R \tag{12b}$$

Table 2 Estimated computer requirements for HSD mechanization approaches

Mechanization approach	Estimated computer requirements: Storage	Duty cycle
1) Series expansion	4 (most)	4 (most)
2) Empirical curve-fitting polynominal	3	3
3) Reference-point integral	2	2
4) Reference-point differential	1 (least)	1 (least)

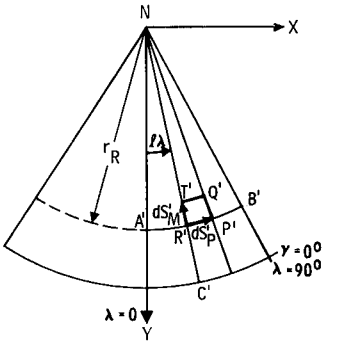

Fig. 6 Lambert Conformal projection.

$$c = \tfrac{1}{6}(1 + f) \tag{12c}$$
$$d = \tfrac{1}{24}[5(\sin\gamma_R - 0.8l) + 3(\sin\gamma_R - l/3)f]/\cos\gamma_R \tag{12d}$$
$$f = 4(\sin\gamma_R - l/2)b/\cos\gamma_R \tag{12e}$$

so that the 1st-, 2nd-, 3rd-, and 4th- order equations of Eq. (11) are defined by the number of terms included in the series.

The HSD mechanizations using Eqs. (9) and (11) are designated as configurations A, B, C, or D, according to the highest order of $\Delta\gamma$ being 1, 2, 3, or 4, respectively.

Mechanization

Map radius determination

Equations (9–12) are used for mechanizing the computation of map radius. They provide adequate accuracy to meet requirements listed in Table 1 with reasonable computer storage and duty cycle. [A comparison with Eqs. (1) and (2) indicates the dramatic simplification.]

Present position x and y translation

The HSD Transparency is commanded to move in x and y directions, so that the aircraft present position on the chart image is centered on the viewing screen.

By definition, as shown in Fig. 7, the reference meridian coincides with the y axis and the reference parallel is tangent to the x axis. Thus, the coordinates of the present position P with respect to the reference point R are

$$x_p = r_{PT}\sin(l\Delta\lambda)$$
$$y_P = r_{PT}\cos(l\Delta\lambda) - r_{RT} \tag{13}$$

where r_{PT} and r_{RT} are the transparency map radii at the present position and the reference point, and they are related to the corresponding Lambert projection map radii as follows:

$$r_{PT} = k_r k_{cs} r_P \tag{14}$$
$$r_{RT} = k_r k_{cs} r_R \tag{15}$$
$$\Delta\lambda = \lambda_P - \lambda_R \tag{16}$$

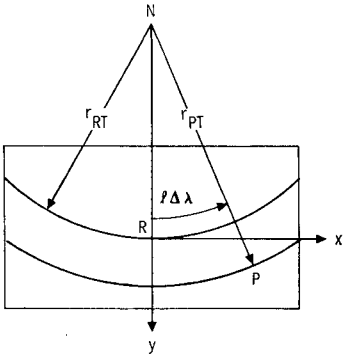

Fig. 7 Transparency coordinate axes.

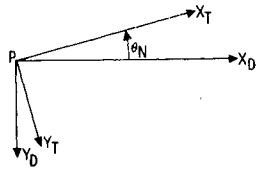

Fig. 8 Definition of chart image rotation angle.

Equation (13) provides the transparency x and y translation mechanization equations.

Image rotation

In north-up display (Fig. 1) the north direction of the chart image with respect to the aircraft present position is aligned with the display index. This can be accomplished through a clockwise rotation of an angle $l\Delta\lambda$ about the aircraft present position P. If the chart image rotation angle is positive counter-clockwise as shown in Fig. 8, then the chart image rotation command is

$$\theta_N = -l\Delta\lambda \tag{17}$$

In Fig. 8, x_T and y_T represent the orientation of the coordinate axes of the transparency image; x_D and y_D, that of the display coordinate axes. When the aircraft present position and the reference point coincide, so do the x_T, y_T and x_D, y_D axes. For a heading-up display, the aircraft true heading is simply added to the north-up image rotation command.

Necessary input (stored) map data

Generally, five input parameters are required to identify each Lambert Conformal projection chart transparency, e.g., 1) two standard parallels γ_1 and γ_2, 2) one chart scale k_{cs}, and 3) two reference point coordinates γ_R and λ_R.

Because of the map radius mechanization used, only four input parameters are required. They are γ_0, r_{RT}, γ_R, and λ_R. The characteristics represented by γ_1, γ_2, and k_{cs} are imbedded in those represented by γ_o and r_{RT}, where $r_{RT} = k_r k_{cs} r_R$.

Computational flow

Figure 9 presents the block diagram of a possible HSD mechanization describing HSD input data, mechanization equations, and output commands. Note that configuration B (second order Taylor's series) is assumed. It is seen that much of the computation is required only upon changing transparencies. As previously noted, x, y map locations for additional points of interest can be computed in the same manner as the map drive parameters.

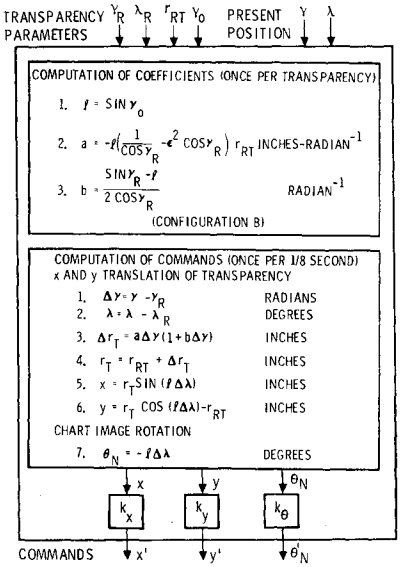

Fig. 9 Block diagram of HSD mechanization.

Table 3 HSD transparencies used for evaluation

Chart series	No. of samples	Chart scale
JN	4	$1{:}2 \times 10^6$
ONC	9	$1{:}1 \times 10^6$
Sectional	10	$1{:}0.5 \times 10^6$

A possible HSD mechanization logic configuration for computing and outputting the command signals is shown in Fig. 10. Each time a new transparency is selected to be displayed on the viewing screen, the initial entry is executed and a new set of four transparency parameters (γ_R, λ_R, r_{RT}, γ_o) is stored, and three map radius equation coefficients (l, a, b) for the transparency are computed and stored. These parameters and coefficients are then subsequently used to compute the command signals.

If there is no change in the transparency selection, the normal entry is executed and the parameters and coefficients stored during the execution of the initial entry are used to compute the command signals. Based upon this 8/sec computation rate, this mechanization demands only approximately 0.4% duty cycle of a modern airborne digital computer.

IV. Error Analysis

In this section, an error analysis of the x and y servo drive mechanization (Fig. 9) is presented

$$x = r_T \sin(l\Delta\lambda),\ y = r_T \cos(l\Delta\lambda) - r_{RT} \tag{18}$$

where

$$r_{RT} = k_r k_{cs} r_R \tag{19}$$

The error analysis presented in this section is also applicable to the symbol placement. Errors due to the image rotation computation [Eq. (17)] are straightforward and less critical so are not discussed here. HSD hardware errors are not included in this discussion.

Error Model

Figure 11 presents the block diagram of an error model for the x and y servo drives. It is based on the HSD mechanization described in Sec. III.

Error sources

There are four major error sources; 1) r_{RT} quantization error $e_{r_{RT}}$, 2) γ_0 quantization error e_{γ_0}, 3) Δr mechanization error e_{Δ_r}, and 4) x and y quantization errors e_{qx} and e_{qy}.

The input quantization errors $e_{r_{RT}}$ and e_{γ_0} are caused by the finite quantizing steps used in the computer to store the input parameters r_{RT} and γ_o, respectively. As an example, for the 16-bit word length to store a signed value, the quantizing step is equal to 2^{-15} of the maximum magnitude. The mechanization error e_{Δ_r} is that caused by using the simplified Eq. (11). The output quantization errors e_{qx} and e_{qy} are also caused by finite quantizing steps.

Error definition

The relative error e is defined as the ratio of the HSD mechanization display error (expressed in inches on display screen) to the display screen diameter d say 6 in. It is mainly composed of four relative error components caused by their respective error sources

$$e = \sum_{i=1}^{4} e_i \tag{20}$$

where

$$e_i = f(\text{error source } i \text{ as previously defined}) \quad (21)$$

Error Sensitivities

The functional relationships of $e_i (i = 1, 2, 3, 4)$ in Eq. (21) must be determined before numerical computation can be performed upon Eq. (20). First, the general expression for the error sensitivities relating e_i to their respective error sources $S (S = r_{RT}, \gamma_o, \Delta r_T, \text{and } e_q)$ are derived. Then, specific expressions are obtained by using appropriate parameters.

General expression of error sensitivities

The x and y servo drive equations can be rewritten as follows:

$$\begin{aligned} x &= (r_{RT} + \Delta r_T) \sin l\Delta\lambda \\ y &= (r_{RT} + \Delta r_T) \cos l\Delta\lambda - r_{RT} \end{aligned} \quad (22)$$

Partial differentiation of Eqs. (22) with respect to S yields the error sensitivity coefficients

$$\begin{aligned} \partial x/\partial S &= (\partial/\partial S)[(r_{RT} + \Delta r_T) \sin l\Delta\lambda] \\ \partial y/\partial S &= (\partial/\partial S)[(r_{RT} + \Delta r_T) \cos l\Delta\lambda - r_{RT}] \end{aligned} \quad (23)$$

Let e_x and e_y be the servo drive error along the x and y axes, and they are related to error in $S(e_S)$ as follows:

$$e_x = (\partial x/\partial S)e_S, \; e_y = (\partial y/\partial S)e_S \quad (24)$$

and

$$(e_x^2 + e_y^2)^{1/2} = [(\partial x/\partial S) + (\partial x/\partial S)^2]^{1/2} e_S \quad (25)$$

The relative error caused by S can be written

$$\begin{aligned} e_i &= (k_m/d)[e_x^2 + e_y^2]^{1/2} \\ &= \frac{k_m}{d}\left[\left(\frac{\partial x}{\partial S}\right)^2 + \left(\frac{\partial y}{\partial S}\right)^2\right]^{1/2} e_S \\ &= (\partial e_i/\partial S)e_S \end{aligned} \quad (26)$$

where

$$\partial e_i/\partial S = (k_m/d)[(\partial x/\partial S)^2 + (\partial y/\partial S)^2]^{1/2} \quad (27)$$

Equation (27) provides the general expression of the error sensitivities relating e_i $(i = 1, 2, 3, \text{and } 4)$ to the error sources $S (S = r_{RT}, \gamma_0, \Delta r_T, \text{and } e_q)$, respectively.

Relative errors vs error sources

By substituting appropriate parameters into Eqs. (26) and (27), the relative errors vs their respective error sources can be written as follows:

$$\begin{aligned} e_1 &\leq (k_m w/dr_{RT})e_{rRT} \\ e_2 &\leq (k_m w/d \tan\gamma_o)e_{\gamma_0} \\ e_3 &= (k_m/d)e_{\Delta rT}, \; e_4 = (k_m/d)e_q \end{aligned} \quad (28)$$

where $w = \frac{1}{2}$ transparency width $\cong r_{RT}(l\Delta\lambda_{\max})$, d = display diameter.

Error Distribution

The maximum and rms error values for each of the sources can be developed as follows.

r_{RT} input quantization

Using the rounding-off technique, the maximum value of the r_{RT} quantization is equal to one-half of the quantizing step

$$(e_{rRT})_{\max} = q_{rRT}/2 \quad (29)$$

Assuming the quantization error in r_{RT} varies with equal probability from zero to its maximum value, the rms of e_{RT} can be written as follows:

$$\langle e_{rRT}^2\rangle^{1/2} = [\tfrac{1}{3}(e_{rRT})^2_{\max}]^{1/2} \quad (30)$$

γ_o input quantization

Similar to r_{RT} quantization, the maximum and rms errors of γ_0 quantization can be written as follows:

$$(e_{\gamma o})_{\max} = q_{\gamma_0}/2 \quad (31)$$

$$\langle e_{\gamma o}^2\rangle^{1/2} = [\tfrac{1}{3}(e_{\gamma o})^2_{\max}]^{1/2} \quad (32)$$

Δr_T mechanizatian

The error of Δr_T mechanization can be written with the aid of Eqs. (2, 9, and 11) as follows:

$$e_{\Delta rT} = k_{cs}k_r[(r_R + \Delta r) - r] \quad (33)$$

where

$$\begin{aligned} r &= Ke^{-l\tau} \\ \Delta r &= a\Delta\gamma[1 + b\Delta\gamma + c(\Delta\gamma)^2 + \ldots] \end{aligned}$$

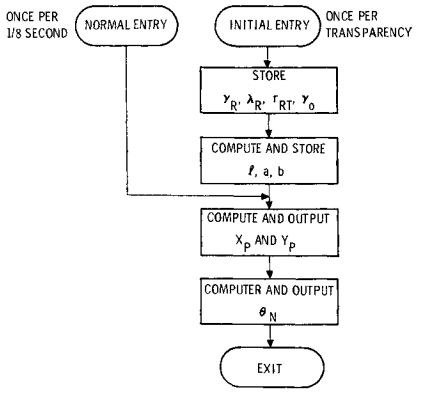

Fig. 10 HSD mechanization logic (configuration B).

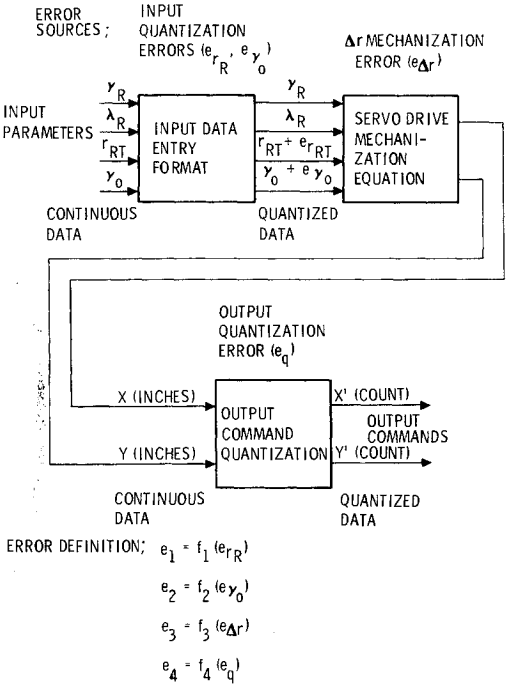

Fig. 11 Error model, sources, and definitions.

Table 4 Maximum error (%), HSD mechanization evaluation

Chart series	No. of samples	A	B	C	D
JN	4	5.383	1.020	0.435	0.429
ONC	9	3.634	0.394	0.284	0.284
Sectional	10	1.168	0.280	0.236	0.236
	rms of 23 maxima	2.507	0.485	0.282	0.282

Table 5 The rms error (%), HSD mechanization evaluation

Chart series	No. of samples	A	B	C	D
JN	4	1.802	0.422	0.223	0.223
ONC	9	1.316	0.197	0.130	0.152
Sectional	10	0.228	0.132	0.130	0.130
	rms of 23 rms's	1.125	0.237	0.158	0.158

For each chart transparency, $e_{\Delta r_T}$ is zero at the reference point, increases as $\Delta\gamma$ increases, and is maximum at either of the two latitude extremes on the transparency.

The rms error is computed as follows:

$$\langle e^2_{\Delta r_T}\rangle^{1/2} = \left(\frac{1}{N}\sum_{p=1}^{N} e^2_{\Delta r_{Tp}}\right)^{1/2} \tag{34}$$

where N is a sufficiently large number. p is a random sample point on the transparency.

x and y output quantization

The output quantization error due to the x and y quantization errors e_{qx} and e_{qy} can be expressed as follows:

$$e_q = (e_{qx}{}^2 + e_{qy}{}^2)^{1/2} \tag{35}$$

The maximum and RMS values can be written as follows:

$$(e_q)_{\max} = [(e_{qx})_{\max}{}^2 + (e_{qy}{}^2)_{\max}]^{1/2} \tag{36}$$

$$\langle e_q{}^2\rangle^{1/2} = [\langle e_{qx}{}^2\rangle + \langle e_{qy}{}^2\rangle]^{1/2} \tag{37}$$

where, as before

$$(e_{qx})_{\max} = qx/2, \quad (e_{qy})_{\max} = qy/2 \tag{38}$$

$$\langle e_{qx}{}^2\rangle^{1/2} = (1/3^{1/2})(e_{qx})_{\max}, \ \langle e_{qy}{}^2\rangle^{1/2} = (1/3^{1/2})(e_{qy})_{\max} \tag{39}$$

Statistical Combination

If e_i's are assumed to be statistically independent random variables with zero means, then the following statistical properties can be deduced from Eq. (20).

Mean of squared value of errors

Let the subscript indices i, j, and k, be defined as follows: i refers to ith error source, $i = 1, 2, 3, 4$; j refers to jth transparency, $j = 1, 2, \ldots m$; and k refers to kth configuration, $k = \text{A, B, C, D}$. Then the mean of square value of the relative error given in Eq. (20) for jth transparency and kth configuration is defined as follows:

$$\langle e^2_{jk}\rangle = \sum_{i=1}^{4} \langle e^2_{ijk}\rangle \tag{40}$$

where

$$\langle e^2_{ijk}\rangle = \text{mean of square value of } \langle e^2_{ijk}\rangle \tag{41}$$

It follows from Eq. (40) that the mean of squared value of the relative error for the kth configuration is defined as follows:

$$\langle e_k{}^2\rangle = \frac{1}{m}\sum_{j=1}^{m}\langle e^2_{jk}\rangle = \frac{1}{m}\sum_{j=1}^{m}\sum_{i=1}^{4}\langle e^2_{ijk}\rangle \tag{42}$$

Root of mean of squared (rms) value of error

Taking square root of Eqs. (40) and (42) yields their respective rms values:

$$\langle e^2_{jk}\rangle^{1/2} = \left[\sum_{i=1}^{4}\langle e^2_{ijk}\rangle\right]^{1/2} \tag{43}$$

$$\langle e^2_k\rangle^{1/2} = \left[\frac{1}{m}\sum_{j=1}^{m}\langle e^2_{jk}\rangle\right]^{1/2} = \left[\frac{1}{m}\sum_{j=1}^{m}\sum_{i=1}^{4}\langle e^2_{ijk}\rangle\right]^{1/2} \tag{44}$$

Mean of squared maximum value of error

Corresponding to Eq. (42), the mean of squared maximum value of the relative error for the kth configuration is defined as follows:

$$\langle e^2_{\max\, k}\rangle = \frac{1}{m}\sum_{j=1}^{m} e^2_{\max\, jk} = \frac{1}{m}\sum_{j=1}^{m}\sum_{i=1}^{4} e^2_{\max\, ijk} \tag{45}$$

where

$$e_{\max\, ijk} = \text{maximum value of } e_{ijk}$$

Root of mean of squared maximum value of error

Taking the square root of Eq. (45) yields the rms maximum value of error

$$\langle e^2_{\max\, k}\rangle^{1/2} = \left(\frac{1}{m}\sum_{j=1}^{m} e^2_{\max\, jk}\right)^{1/2} = \left(\frac{1}{m}\sum_{j=1}^{m}\sum_{i=1}^{4} e^2_{\max ijk}\right)^{1/2} \tag{46}$$

Evaluation Program

In order to evaluate mechanization accuracies, FORTRAN programs were employed. One portion of the program was developed to assess the alternate Δr_T computation configurations (A–D) for various scales and latitude regions by comparing resulting map locations against the reference locations [given by Eqs. (1) and (2)].

In addition, other portions of the program were employed to compute the various quantization errors and to assemble the statistical combinations of error sources, transparencies and configurations described in the previous section for over-all error assessment.

Discussion of Results

Twenty-three transparency samples were selected for the mechanization evaluation representing a spectrum of map scales and central latitudes. These are summarized in Table 3.

The maximum errors resulting from using these 23 transparencies and the HSD mechanization configurations A,

B, C, and D, are listed in Table 4. The rms errors are listed in Table 5. It was found that the various quantization errors were sufficiently small, even for 16-bit word storage and that the over-all errors were dictated by the Δr_T mechanization configuration alternates.

Tables 4 and 5 provide immediate accuracy comparisons relative to the number of terms included in the mechanization equation. This feature enables the user to select a degree of complexity consistent with his particular accuracy constraints. Considering normal limitations of electromechanical-optical hardware, as well as typical operational needs, it is anticipated that the bulk of system applications would point to configurations A and B (1st or 2nd order).

V. Conclusions

A transformation technique, based upon an application of Taylor's Series to the conformality differential equations, has been developed to relate directly Earth latitude and longitude to the x, y map dimensions for a Lambert Conformal projection. Accordingly, it is convenient to directly tradeoff mechanization accuracy against computational complexity for any particular application. The technique also requires a minimum of map-definition parameters that must be entered into and stored within the computer. Further, computations are arranged so that basic map-dependent parameters are computed only at each map change, thus simplifying the high-frequency computations dependent upon aircraft position changes.

The evolved mechanization technique resulted from a system engineering effort, wherein the specialized disciplines of system requirements definition, analysis, computer software organization, and mechanization synthesis were organized for application to the requirement task. The resulting optimized mechanization points up the advantage of the parallel (team) approach to software engineering, rather than a series approach, in an application such as this which tightly couples the various technical and organizational disciplines involved.

Reference

[1] Thomas, P. D., "Conformal Projection in Geodesy and Cartography," Special Publication No. 251, 1964, U.S. Government Printing Office, Washington, D.C.

SYNOPTIC: Higher-Order Control System Dynamics and Longitudinal Handling Qualities, D. A. DiFranco, Cornell Aeronautical Laboratory, Buffalo, N.Y.; *Journal of Aircraft*, Vol. 7, No. 5, 1970, pp. 457–464.

Aircraft Subsystem Design; Aircraft Handling, Stability, and Control; Aircraft Landing Dynamics; Aircraft Testing

Theme

This paper describes an experimental investigation of the effects of higher-order control system dynamics on the longitudinal handling qualities of a fighter airplane. This research used the USAF/CAL variable stability T-33 airplane as an in-flight simulator. Comments and pilot ratings were obtained and correlated with an airplane response delay parameter. Fixed-base and in-flight evaluations were also compared.

Content

Control system dynamics, as well as open-loop airplane dynamics, affect the handling qualities of airplanes. Most handling qualities investigations have been concerned with the effects of variations in certain open-loop airplane parameters. This investigation of higher-order control system dynamics is of special interest since modern high performance fighters employ flight control systems that increase the order of the airplane response to pilot stick inputs. The response can become "nonairplane-like" and affect the airplane handling qualities.

This in-flight investigation is based on a similar ground simulator program. In-flight and fixed-base simulation results can therefore be compared. Higher-order response characteristics were simulated by altering the elevator-stick feel system and the elevator actuator dynamics in conjunction with four different sets of longitudinal short-period airplane dynamics. The dynamics of any of the three elements (feel system, actuator, and airplane) could be changed independently of the others. Airplane dynamics were simulated using the response feedback system of the variable stability T-33 airplane. A block diagram of the pilot in-flight closed-loop control is shown in Fig. 1.

A matrix of 40 configurations was established for in-flight evaluation. The matrix was based on three sets of feel system dynamics (fast, medium, and slow), ten sets of actuator dynamics, and four sets of airplane dynamics. Both the order and break point frequency of the simulated actuators were varied. Three sets of longitudinal short-period dynamics were specified and evaluated for a fighter in "up-and-away" flight and one set was specified and evaluated during landing approach. Combinations of control system and airplane short-period responses as high as eleventh order were simulated and evaluated.

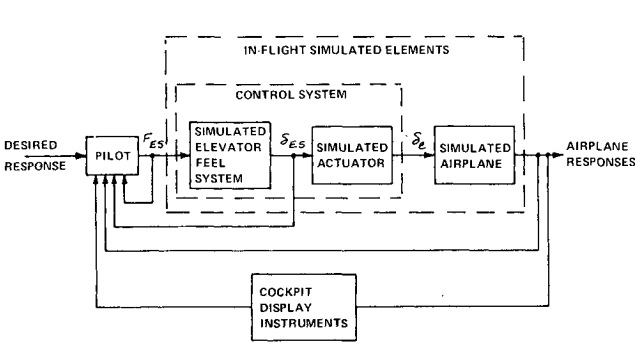

Fig. 1 Longitudinal control loops in flight.

Thirty-six of the configurations were evaluated in-flight by one or both evaluation pilots. The evaluation pilot occupied the front seat and the safety pilot the rear cockpit of the USAF/CAL variable stability T-33 airplane. The evaluation pilot was not informed of the configuration characteristics simulated. Each configuration was evaluated as an all-weather fighter under both VFR and IFR conditions. The landing approach configurations were also evaluated during and ILS approach. The evaluation pilots were asked to make specific comments on each configuration and each configuration was given a pilot rating and a PIO rating.

The pilot comments indicated that as the order was increased and the breakpoint frequency was reduced for the control system elements, the most frequent comment was on the amount of delay or lag in the airplane response following a stick force input. The rapidity of the response after the delay was also considered to be a factor in the closed-loop control difficulties. As the delay increased, precise control and tracking performance continued to deteriorate and then become impossible. PIO tendencies developed just trying to fly the airplane straight and level. Some of the configurations were considered uncontrollable with severe PIO tendencies and given a pilot rating of 10. Although lag was again a source of difficulty to the pilots for the landing approach, most of the deterioration in handling qualities was associated with a degradation of tracking and precise attitude control and not with a development of PIO tendencies.

It is demonstrated in the paper that many of the higher-order responses simulated can be reasonably well represented by a delay and an equivalent second-order response. As an example, the angle of attack (α) and pitch rate ($\dot{\theta}$) transfer functions for elevator stick force (F_{ES}) inputs take the following form:

$$\alpha(S)/F_{ES}(S) = \omega_E^2\,(\alpha/F_{ES})_{SS}\,e^{-\tau s}/(S_2 + 2\zeta_E\omega_E S + \omega_E^2) \quad (1)$$

$$\dot{\theta}(S)/F_{ES}(S) = (\omega_E^2/L_\alpha)\,(S + L_\alpha)\,(\dot{\theta}/F_{ES})_{SS}e^{-\tau s}/(S^2 + 2\zeta_E\omega_E S + \omega_E^2) \quad (2)$$

In Eqs. (1) and (2), τ is the delay time in seconds and ω_E and ζ_E are the equivalent undamped frequency and damping ratio, respectively of the second-order system. The subscript SS refers to the steady-state response.

A method is presented in the paper for determining τ, ζ_E, and ω_E analytically. If the breakpoint frequency of the control system elements are sufficiently higher than the airplane short-period frequency, then the equivalent second-order response will be near the airplane short-period response and the delay time can be determined from the control system phase shift at the short-period frequency using the following formula:

$$\tau = \phi_{CS}/\omega_{SP} \quad (3)$$

ϕ_{CS} is the control system phase shift at the short-period fre-

quency in radians, and ω_{SP} is the short-period frequency in rad/sec.

For most of the configurations simulated a nondimensional delay parameter can be defined in either of the following two ways:

$$\text{Delay parameter} = a/P_E = a/(2\pi/\omega_E) \quad (4)$$

$$\text{Delay parameter} = a/P_{SP} = (\phi_{CS}/\omega_{SP})/(2\pi/\omega_{SP}) = \phi_{CS}/2\pi \quad (5)$$

In Eq. (4), P_E is the equivalent undamped period of the equivalent second-order system. In Eq. (5), P_{SP} is the undamped period of the airplane short period. Equations (4) and (5) are essentially equivalent only when the break point frequency of the control system elements are sufficiently higher than the airplane short-period frequency.

The figures presented in the paper demonstrate that a strong correlation exists between pilot ratings, PIO ratings, and the delay parameter as defined by Eqs. (4) and (5) for all the configurations evaluated. With a degradation in control system dynamics, the delay parameter increases, PIO tendencies increase, and a deterioration in handling qualities occurs. With a delay parameter between 0.2 and 0.26, the control system phase shift increases to between 70° and 90°. The pilot rating becomes 10, the PIO rating becomes 6, and the airplane is considered uncontrollable because of divergent PIO tendencies.

A comparison is made of fixed-base ground simulator vs flight evaluations and this comparison indicates that configurations with significant PIO tendencies are rated poorer in flight than on the ground. In evaluating PIO tendencies, ground simulator results are not conservative and can be very misleading.

Higher-Order Control System Dynamics and Longitudinal Handling Qualities

DANTE A. DIFRANCO*
Cornell Aeronautical Laboratory, Buffalo, N. Y.

An experimental investigation of the effects of higher-order control system dynamics on the longitudinal handling qualities of a fighter airplane are discussed. This research was undertaken using the USAF/CAL variable stability T-33 airplane as an in-flight simulator. Different higher-order responses were simulated by altering the elevator feel system, elevator actuator, and airplane short-period characteristics. Essentially the same configurations were evaluated by two pilots using a revised pilot rating scale. One pilot also rated the configurations for their pilot-induced oscillations (PIO) tendencies. Comments and ratings were related to a response delay parameter. Many of the higher-order control systems investigated produced pronounced PIO tendencies in flight, and some were considered unflyable with certain higher-order characteristics. A comparison of fixed-base and in-flight evaluations indicated that configurations with significant PIO tendencies were rated poorer in flight, and configurations with little or no PIO tendencies were rated better in flight.

Nomenclature

a_i = system delay time (i = LF, ϕ), sec
f_i = frequency (i = a, FS_1, FS_2), cps
F_i = control force (i = ES), lb
g = acceleration of gravity, ft/sec²
$K_1, K_2 \ldots K_n$ = characteristic equation constants
L_α = dimensional lift force derivative with angle of attack, 1/sec
$M_{\delta a}$ = dimensional pitching moment derivative with respect to elevator deflection, 1/sec²
n_z = normal acceleration, g's
n = number of roots or order of characteristic equation
P_i = period (i = E, SP), sec
$PIOR$ = pilot-induced oscillation rating
s = Laplace operator
V = airplane velocity, fps
α = airplane angle of attack from trim level flight, rad
δ_i = control surface or control stick deflection (i = e, ES), rad or in.
ζ_a = damping ratio (i = a, a_1, a_2, E, FS, FS_1, FS_2, p, SP)
θ = airplane pitch angle, rad
$\theta(\text{eta})_\epsilon$ = pitch angle tracking error, deg
ϕ_a = phase angle of control system evaluated at airplane short-period frequency, rad or deg
ω_i = undamped natural frequency (i = a, a_1, a_2, E, FS, FS_1, FS_2, p, SP), rad/sec
$(\dot{})$ = first derivative with respect to time

Subscripts

a, a_1, a_2 = actuator dynamics
e = elevator surface
E = equivalent
ES = elevator stick
FS, FS_1, FS_2 = feel system dynamics
LF = match of lowest-order coefficients in characteristic equation
0 = initial condition
p = airplane phugoid
SS = steady-state value
SP = airplane short period
ϕ = value determined from control system phase shift at airplane short-period frequency

Received July 11, 1969; presented as Paper 69-768 at the AIAA Aircraft Design and Operations Meeting, Los Angeles, Calif., July 14–16, 1969; revision received November 10, 1969. The paper is based on research performed for the Air Force Flight Dynamics Laboratory under Contract AF 33(615)-3294. W. Smith was project engineer for the Flight Dynamics Laboratory.

* Aeronautical Research Engineer, Flight Research Department. Member AIAA.